

Article

# Surface Analysis of Uncoated and PVD Coated Punch at the Hole-Flanging Process

Miroslav Tomáš<sup>1,\*</sup>, Miroslav Džupon<sup>2</sup>, Emil Evin<sup>1</sup> and Emil Spišák<sup>1</sup>

<sup>1</sup> Institute of Technology and Material Engineering, Faculty of Mechanical Engineering, Technical University of Kosice, Mäsiarska 74, 040 01 Košice, Slovakia; emil.evin@tuke.sk (E.E.); emil.spisak@tuke.sk (E.S.)

<sup>2</sup> Institute of Materials Research, Slovak Academy of Sciences, Watsonova 47, 040 01 Košice, Slovakia; mdzupon@saske.sk

\* Correspondence: miroslav.tomas@tuke.sk; Tel.: +421-55-602-3524

Received: 19 February 2018; Accepted: 26 March 2018; Published: 27 March 2018



**Abstract:** This paper researches the surface condition and wear on the hole-flanging punch when producing a flanged Ø7 mm hole in a steel strip S355J2 + N (1.0577) with a thickness of 3 mm. The hole was flanged by a punch with a defined geometry known as a tangent ogive and described via a caliber radius head (CRH) ratio. During the process, wear of the punch made of hardened tool steel 1.3343 appeared after 20,000 strokes. Thus, a multipurpose coating TiCN-MP deposited via Lateral Rotating Arc-Cathode technology was applied on the punch to extend the punch lifetime. The coated punch was polished to remove droplets after deposition process. By applying TiCN-MP coating, 120,000 strokes were applied to reach the same wear as for the uncoated tool steel. The surface of the punch made of the hardened tool steel for uncoated and PVD coated conditions was researched by scanning electron microscopy after wear, and an energy dispersive X-ray (EDX) analysis was done to identify components of bonded material. In addition, the normal pressure on the punch active surface was studied via a numerical simulation of the hole-flanging process. The position of the high normal pressure is well correlated to the position of the adhesive wear for the uncoated and coated punches.

**Keywords:** hole-flanging; punch; PVD coating; TiCN-MP; wear; normal pressure; numerical simulation

## 1. Introduction

Hole-flanging belongs to the forming operations and is used when thin-walled structures are produced in order to make material stock for thread. It is the conventional stamping method for pre-producing the hole by forming material onto the cylindrical or coned collar made from standard or high strength steels, using blank holder and hole-flanging punches [1,2]. Besides conventional hole-flanging processes with or without wall thinning, new methods appeared, such as incremental forming [3,4]. Some limits, such as rapid tool wear and time for tool change, along with maintenance, are connected when conventional methods are used to make the initial hole. Contactless methods, such as drilling via laser-beam with movements along the hole circumference or a direct laser-beam impact to the processed material, appear to be a solution [5,6].

Many previous works have investigated the hole-flanging process from different points of view and using different materials. Stachowicz [7] studied the hole-flanging process on deep drawing steel sheets with a circular hole drilled in the center. He also used punches with different geometries and experimentally determined the effect of both the punch geometry and material mechanical parameters (especially strain hardening and plastic anisotropy) on the expansion limit of the hole. Fracz et al. [8] studied the thickness distribution when different punch shapes were used. Krichen [9] determined

the effect of the blank-holding on sheet aluminum alloys when constant and progressive forces were applied, as well as when no blank holder was used. Fracz and Krichen also used finite element analysis to research the process and to verify constitutive material models via experimental results. Li [10] investigated the effect of mechanical properties on the hole flangeability of stainless steel sheets. He found that the flangeability of stainless steel sheets is strongly dependent on both the work hardening exponent and the material anisotropy. Hole-flanging with cold extrusion presented in [11] avoided necking or fractures during the hole-flanging process, and a substantial flange height and lip thickness could be achieved.

Nowadays, technological processes are investigated via numerical simulations based on a finite elements method. These results show a good agreement between the experimental and simulation results. This resulted from material models developed and implemented in a simulation software and an improvement of experimental measurements' model constants. Huang [12] studied the stretch flanging of circular plates via Lagrangian elasto-plastic finite element method. The results of the punch load, deformed geometry and thickness distribution were verified experimentally. Thipprakmas [13] implemented an FEM (finite elements method) analysis when studying the hole-flanging process for conventional cutting and fine blanking of the initial hole. Thus, they stated better shapes of the flange when fine blanking was used and quantitatively clarified the relationship between the FB-hole-flanging conditions and the flanged shapes. In [2], the author analyzed process parameters related to the flange forming direction, including punching clearance, flange thickness, and hole expansion ratios. Kacem [14] predicted the limits of the hole-flanging process through a physically based approach of damage and of verified FEM results via experiments. The results showed that the model accurately predicts all types of failures (orange peel aspect, necking, microvoids, tear) for different conditions and for both materials that were used. Masmoudi [15] used FEM to analyze the effect of clearance between the die and the punch on the flange height, and they applied a Gurson–Tvergaard–Needleman coupled approach to ensure that the flange was free from fracture. Heng-Sheng [16] used a numerical simulation to find out the parameters that counter pressure dependent on the inner diameter for hole-flanging with cold extrusion.

The operating variables for tribological contact in metal forming depend on the actual application. One important variable is the normal pressure on the die or punch (usually on the radius), where possible wear can occur. The normal pressure varies from 1 to 100 MPa for sheet metal forming processes, and from 100 to 1000 MPa for drawing with ironing [17]. Some results investigated by numerical simulation were also presented in [18] for the deep drawing of automotive parts, as well as in [19] for the strip drawing test, and in [20] for the deep drawing. Pereira experimentally revealed the strong relation between high normal pressure zones corresponding to a severe galling wear mechanism [21].

The wear mechanism in forming processes depends on solid body materials (involving coatings), their relative motion and lubricants. The problem was investigated by Gorscak [22] for uncoated steel when PVD coatings were applied to the tool. Groche [23] performed an investigation on different process parameters on the wear of forming tools when zinc-coated sheet metals are processed. He found that the process parameters corresponding to gliding speed and normal pressure influenced the wear of forming tools. Moravec [24] showed a positive effect of TiCN coating when applied to the cold molding tools. Clarysse et al. [25] studied the resistance to galling and the abrasive wear for selected coatings by means of a flat/cylindrical multifrottement test and cup test. Silva et al. [26] improved the wear resistance of a mold by applying a multilayer nanostructured coating: the lifespan was 65.5 times greater than that of the uncoated substrate. Li [27] studied microstructural, residual stress corrosion and wear resistance for multilayer titanium coatings when deposited on a magnesium alloy.

The surface preparation and droplet elimination after the coating process are important issues for reaching a good tool/coating performance. In the paper [28], a final elimination of droplets by drag grinding was performed and a positive effect was found for some coatings. In [29], microblasting mechanical substrate pre-treatments were analyzed with regard to the performance of coated tools. A drag grinding pre-treatment led to an improvement of the coating adhesion and to a reduction

of wear at the thread tapping process described in [30]. Additionally, indirect methods for seeking common features among the group of cutting tools with the best performances on machining have been presented in [31].

The problem researched in our paper arose when hole-flanging was designed and used in the production of a flange for a self-tapped screw in a structural part of the trailer. The aim of the article is to study the surface condition and wear on the hole-flanging punch when it is made of hardened tool steel without and with PVD coating. In addition, the normal pressure on the punch active surface was studied via a numerical simulation of the hole-flanging process. We suppose that the PVD coating improves the tool life, thus shortening the maintenance time.

## 2. Materials and Methods

The experiments focused on the hole-flanging process of structural steel S355J2 + N (1.0577) with a thickness of 3 mm. The geometry of the punch and die is shown in Figure 1. The initial  $\text{\O}3$  mm hole is cut by a CO<sub>2</sub> TruLaser 3040 laser (Trumpf, Ditzingen, Germany) with the following parameters: Power at 3 kW; switching frequency at 2000 Hz; speed at 4.5 m·min<sup>-1</sup>; offset at 0.7 mm; gas and gas pressure at O<sub>2</sub>/0.6 bar; and corner cooling time of 0.5 s.

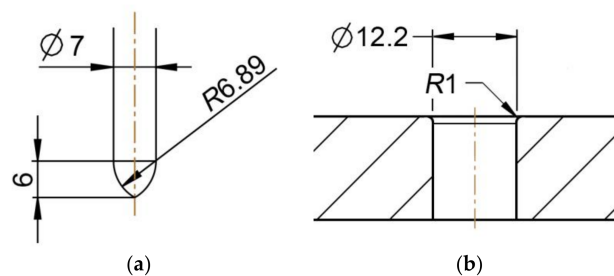


**Figure 1.** The geometry of hole-flanging forming die: (a) Punch; (b) die.

The chemical composition of the steel is shown in Table 1. The mechanical properties are shown in Table 2.

**Table 1.** The chemical composition of steel S355J2 + N (wt %).

C	Mn	P	S	Si	Al	Nb	Ti
0.065	0.76	0.007	0.004	0.023	0.038	0.026	0.002

**Table 2.** The mechanical properties of steel S355J2 + N.

Spec. No.	$Re_H$ (MPa)	$Re_L$ (MPa)	$Rm$ (MPa)	$A_g$ (%)	$A_{80}$ (%)
1	379	374	554	15.5	27.0
2	386	378	561	15.6	29.4
3	375	372	554	15.6	29.3
Average	380	374	556	15.6	28.5
Standard deviation	4	2	3	0	1.1

The punch was made of tool steel 1.3343, heat treated via vacuum hardening and tempered to 61 HRC. The punch surface was machined by grinding and polished to a final roughness of Ra 0.2  $\mu\text{m}$ . The surface topography was inspected with the raster electron microscope JEOL JSM-7000F. The chemical composition of the tool steel is shown in Table 3.

**Table 3.** The chemical composition of tool steel 1.3343 (wt %).

C	Si	Mn	P	S	Cr	Mo	V	W
0.92	0.31	0.33	0.019	0.005	3.88	4.76	1.85	6.36

PVD coating TiCN-MP was deposited via LARC (Lateral Rotating Arc-Cathode) technology. The main process parameters were as follows: Bias 160 V, ARC Ti-180 A, pressure 0.008 mbar, temperature 430 °C. The chemical composition of the coating was measured via Glow Discharge Optical Emission Spectroscopy (GD-OES, Leco Instrument, Joseph, MI, USA) as deep level concentration profiles. The phase composition of the coating was examined via a grazing incidence X-ray diffraction method (Bruker AXS GmbH, Karlsruhe, Germany). All records of the qualitative phase analysis were measured with an impact angle of 2°, within an interval of 20° to 100°.

The Calotest method was used to measure the coating thickness. The indentation microhardness was measured via tester TTX-NHT S/N (Anton Paar GmbH, Graz, Austria) with a diamond indenter Berkovich at a maximal load of 60 mN and a sinus mode (frequency 15 Hz, amplitude 6 mN and holding time at max. load 10 s).

The surface topography was measured via an optical method of confocal microscopy and optical interferometry, with a phase shift interference (PSI) regime, a vertical resolution of PSI <0.02 nm and a control length 636 µm. The surface topography was also verified via the electron microscope JEOL JSM-7000F (JEOL Ltd., Tokyo, Japan) and Vega3 Tescan microscope (TESCAN Brno, s.r.o., Brno, Czech Republic). Scanning electron microscopy (SEM) analyses were done using a secondary electron (SEI) regime, with a bias of 10 kV and a work distance of 10 ± 2 mm from the sample surface.

The adhesion of TiCN-MP coating to the hardened tool steel was identified via a Micro-Scratch test with a linear increase of the normal force  $F_z$  to −120 N. The test was done using the device UMT/APEX Multi-Specimen (Bruker, Campbell, CA, USA) with a diamond Rockwel indenter and a sample speed of 0.01 mm·s<sup>−1</sup>. The adhesion properties of the coating system were evaluated from the view of the scratch line morphology, fracture of the coating on the scratch line-coating edge, as well as from the graphic records of the acoustic emission AE and the friction coefficient COF, both depending on a normal force  $F_z$ .

The friction coefficient of the coating was measured via a Pin-On-Disc test on the tribometer CSM HT device (CSM Instruments, Needham, MA, USA). During the test, a hardened Ø6 mm steel ball was used, and loads of 2, 4 and 5 N were applied. The speed was 20 cm·s<sup>−1</sup> and sliding distance 200 m.

A numerical simulation of the hole-flanging process was done in the software Pam Stamp 2G, commonly used when forming processes are simulated. A surface CAD model was created according to the punch and die dimensions (Figure 1). Following this, it was imported and meshed via a DeltaMesh module with the size of the elements between 0.1 and 30. These parts were defined as a Rigid Body; no elastic deformation was therefore allowed.

The model of the processed material was constituted via a Hill 48 yield condition and Krupkowsky strain hardening equation. The values of the constant were calculated from the results of the tensile test via ISO 6892-1, as shown in Table 2. Due to material thickness, the volume blank was defined and meshed in thickness onto 5 layers with an element size of 0.35 mm. Thus, hexahedron volume elements were created.

A Coulomb friction condition was set with a friction coefficient ranging from 0.3 (the value specified by the software manual) to the maximal values measured on the Pin-On-Disc test. The contact pressure on the punch surface was evaluated in 10 states during the punch path in order to identify the maximal contact pressure.

### 3. Results and Discussion

#### 3.1. Punch without Coating

The surface and wear of the punch hardened and tempered to 61 HRC was researched after 1500 and 7000 flanged holes were produced. The distinctive wearing was shown on a punch after 7000 flanged holes (Figure 2a). The active punch surface (punch tip) was created by a tangent ogive with the following parameters: punch diameter  $D = 7$  mm,  $R = 6.89$  mm,  $L = 6$  mm, as shown

in Figure 2b. Based on [32] the ogive is described by the  $CRH$  parameter calculated as follows:  $CRH = R/D = 6.89/7 = 0.98$ .

The SEM method was used to check the punch after 1500 and 7000 strokes (flanged holes). On the punch surface, after 1500 strokes, no wear was identified in the ogive area and the cylindrical punch part; the surface was compact in both areas (Figure 3). Some alloying elements from tool steel 1.3343 were identified via a qualitative EDX (energy dispersive X-ray) microanalysis in the ogive area, transition ogive-cylinder area and in the cylindrical part of the punch. The ogive profile of the punch tip showed a minor change to the conical surface without any subsurface plastic deformation (Figure 3b).

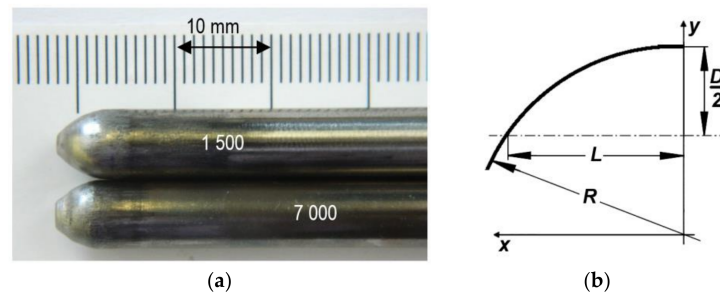


**Figure 2.** Punches after wearing: (a) Punches after hole-flanging; (b) the tip geometry.

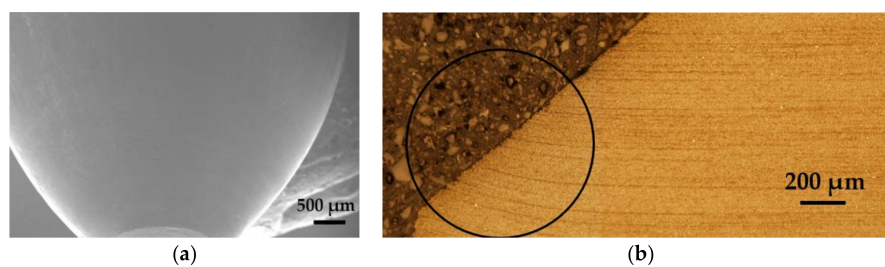


**Figure 3.** The active punch surface after 1500 strokes: (a) SEM (scanning electron microscopy) analyse; (b) profile.

The analysis of the punch surface after 7000 strokes (flanged holes) showed the intensive adhesive wear of the ogive area, as shown in Figure 4. The qualitative EDX analysis in the ogive area (Figure 4a) detected that only elements included in the material S355J2 + N and any alloying elements from tool steel 1.3343 had been found. The detailed EDX analysis (the rectangle shown in Figures 4a and 5) showed intensive galling of the base material and its release by the tool movement. The punch profile in the ogive area was formed by wear into a conical shape (Figure 4b). The change of the punch profile corresponds to the papers [33,34], which focused on the analysis of spherical, conical and cylindrical punch shapes. They stated the lowest maximal load for a conical punch shape when flanging the hole [12,13].

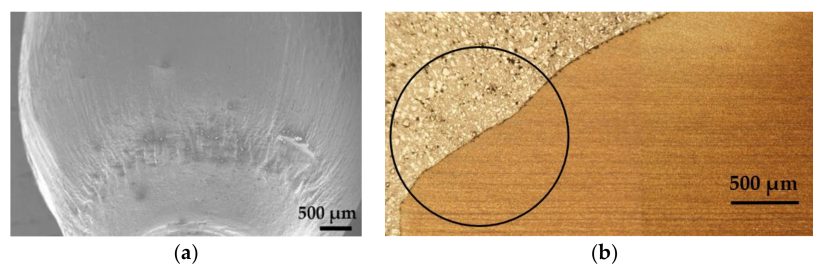


**Figure 4.** The active punch surface after 7000 strokes: (a) SEM analyse; (b) profile.

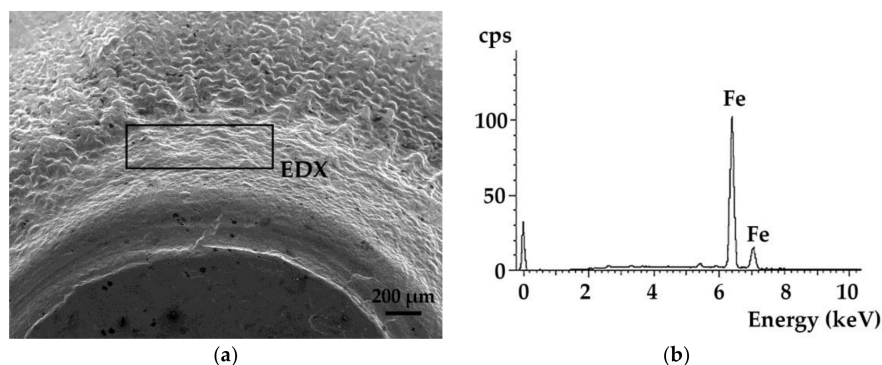


**Figure 5.** The detailed EDX (energy dispersive X-ray) analysis of the ogive punch surface: (a) SEM analyse; (b) EDX spectra.

### 3.2. Punch with TiCN-MP Coating

The thickness of the coating was 2.51  $\mu\text{m}$ , and the average value of the indentation microhardness  $H_{IT}$  was 54 GPa. The GD-OES analysis identified Ti, N and C elements in the PVD coating. The measurements were done at a depth of 5  $\mu\text{m}$  (Figure 6a). Using a grazing incidence X-ray technique, only phases of the Face Centered Cubic type were found: FCC–Fm3m (225) with crystallites sizes of  $6.8 \pm 2$  nm (Figure 6b).

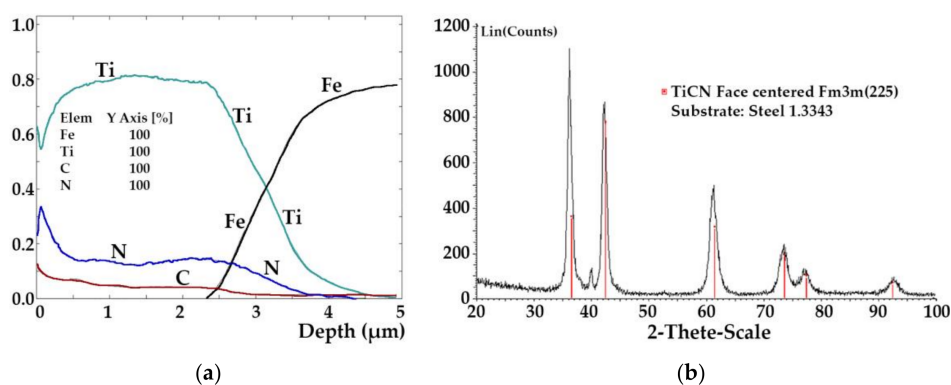


**Figure 6.** An analysis of the TiCN-MP coating deposited on substrate 1.3343 with 61 HRC: (a) GD-OES analysis; (b) GI qualitative X-ray analysis.

The roughness values of the TiCN-MP coating deposited on the tool steel were measured five times. The roughness  $Ra$  was directionally dependent, as shown in Table 4. The surface roughness 3D parameters  $S_p$ ,  $S_v$ , and  $S_z$  involved extreme values of profile height resulting from the random occurrence of isolated particles on the test area, as documented below. These parameters were used to detail the characterization of the coating surface, in addition to the  $Ra$  value.

The average friction coefficients, from 0.495 to 0.780, were measured via a Pin-On-Disc test on three samples for each testing condition. These values did not show the change for each normal force set during the test (Table 5).

**Table 4.** The parameters of the surface microgeometry of the TiCN-MP coating ( $\mu\text{m}$ ).

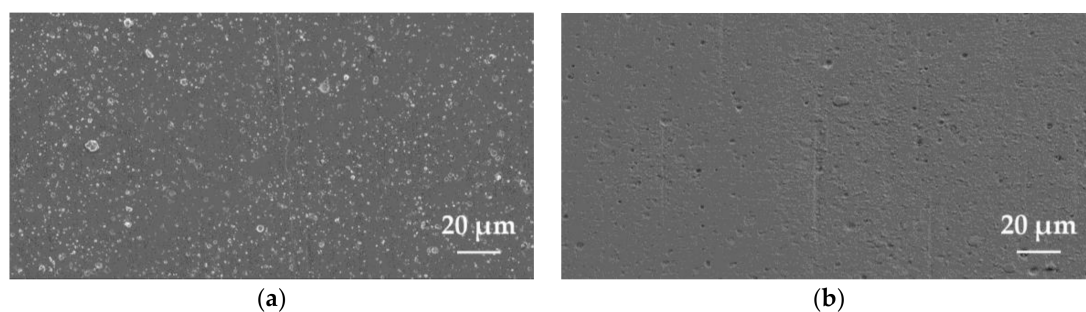
Statistical Variables	ISO 25 178				ISO 4287		
	$S_q$	$S_p$	$S_v$	$S_z$	$S_a$	$Ra\text{-long}^1$	$Ra\text{-trans}^1$
Average	0.44	4.06	2.34	6.39	0.35	0.170	0.140
Standard deviation	0.06	0.55	0.16	0.22	0.04	0.003	0.002

<sup>1</sup> Long—measured in the grinding direction, Trans—measured normal to the grinding direction.

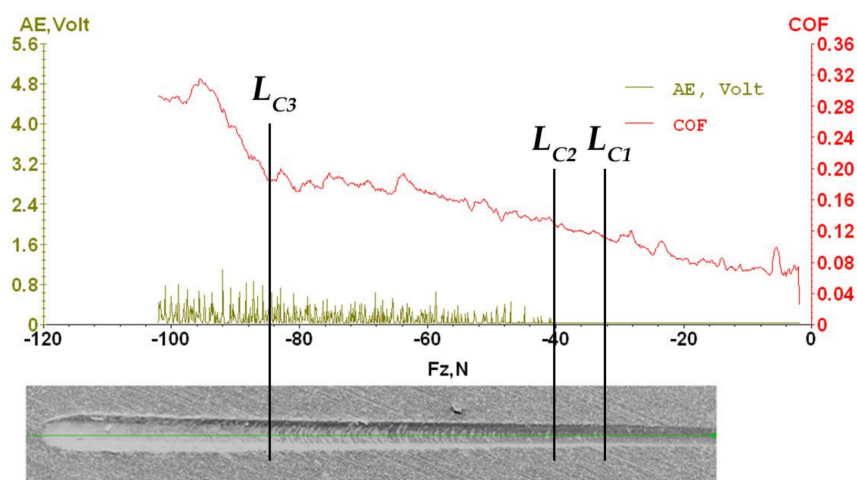
**Table 5.** The friction coefficient measured via Pin-On-Disc test.

$\mu$ -Mean (-)	$\mu$ -StDev (-)	$F$ (N)	$v$ (cm·s <sup>-1</sup> )	Distance (m)
0.780	0.076	2	20	200
0.700	0.029	4	20	200
0.495	0.066	5	20	200

A scan electron microscope was used to verify the coating surface morphology. No fracture was found in the coating TiCN-MP, but globular particles of different sizes (Figure 7a) were detected on the surface. An EDX analysis of the particles detected a Ti component. The presence of globular Ti particles on the coating surface is a result of a deposition process via the LARC technology. The number and size of the macroparticles depend mainly on the parameters of deposition as well as on the deposited material. Based on [28,29], the post-treatment of the coating is crucial to avoid droplets, which are the main cause of coating failure. Thus, a PVD coated punch was polished to remove them (Figure 7b).

**Figure 7.** The surface of the TiCN-MP coating identified via SEM: (a) After coating; (b) after drag grinding.

The result of the Micro-Scratch test is shown in Figure 8 and seven tests were performed. The acoustic emission signal gradually increased, the signal intensity was low and no step change was found when increasing the normal force. Concerning the morphology change of the scratch line's edge and bottom, identified via the SEM method and the EDS LineScan analysis, the cohesive failure was found at the force  $L_{C1} = 34.7 \pm 4.0$  N. Adhesion failure and spallation of the coating was found at the force  $L_{C2} = 41.6 \pm 2.6$  N and critical force to surface exposure at the center of the track  $L_{C3} = 86.1 \pm 2.9$  N was found.

**Figure 8.** The record of the Micro-Scratch test and scratch track; AE-Fz, COF-Fz (AE—acoustic emission, COF—coefficient of friction, Fz—normal force).

Residual stresses involved in the coating after the PVD process are very important. An X-ray phase analysis yielded qualitative information and the orientation of deformation. The phase composition of the coating was determined via a grazing incidence X-ray diffraction method with an impact angle  $2^\circ$  within an interval of  $20^\circ$  to  $100^\circ$ . For the TiCN-MP coating deposited on the tool steel 1.3343 and hardened to 61 HRC, a negative value of deformation  $\varepsilon = -0.017$  was measured. The deformation was calculated via a multi-hkl method from GI measurements. A negative value implies a compression in the TiCN-MP coating, and it was parallel to the surface.

The wear of the punch coated with the TiCN-MP layer after 120,000 working cycles was localized onto the ogive area of the punch, as seen in Figure 9. The EDX analyses in points 1 and 3 detected an Fe component, and no alloying elements from tool steel 1.3343 (Cr, Mo, V, W) were found (Figure 10a,c). Thus, the transfer of the processed material onto the punch ogive surface, known as galling, appeared. The TiCN-MP coating in the cylindrical part of the punch was compact, as shown in Figure 10c.

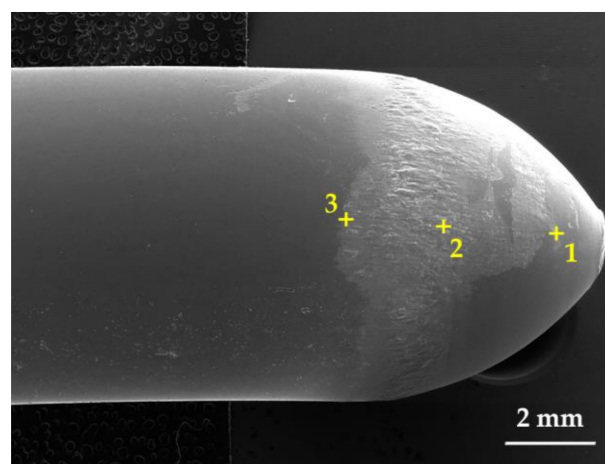


Figure 9. The punch surface after 120,000 strokes.

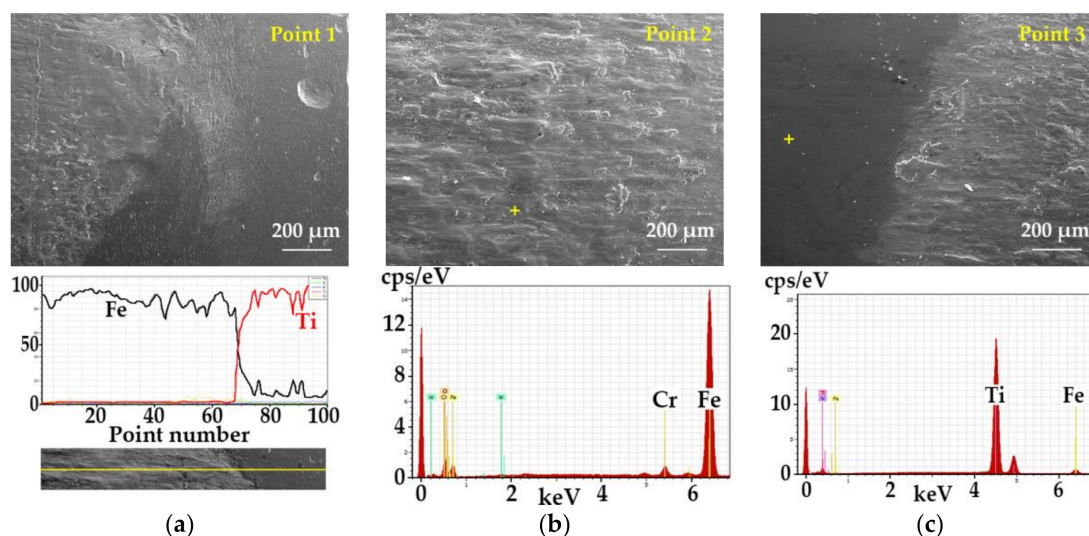
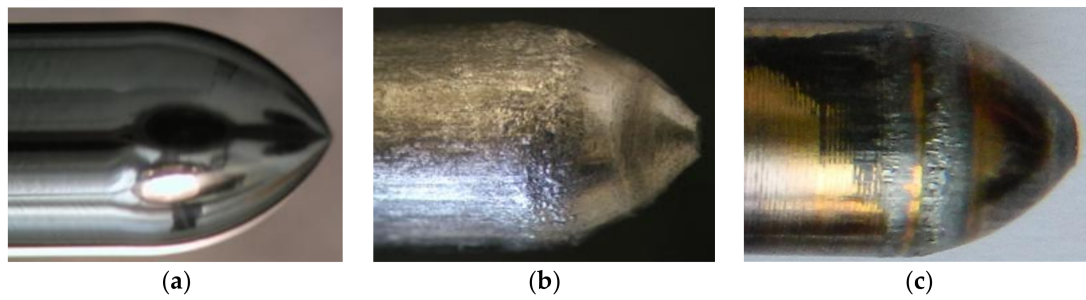
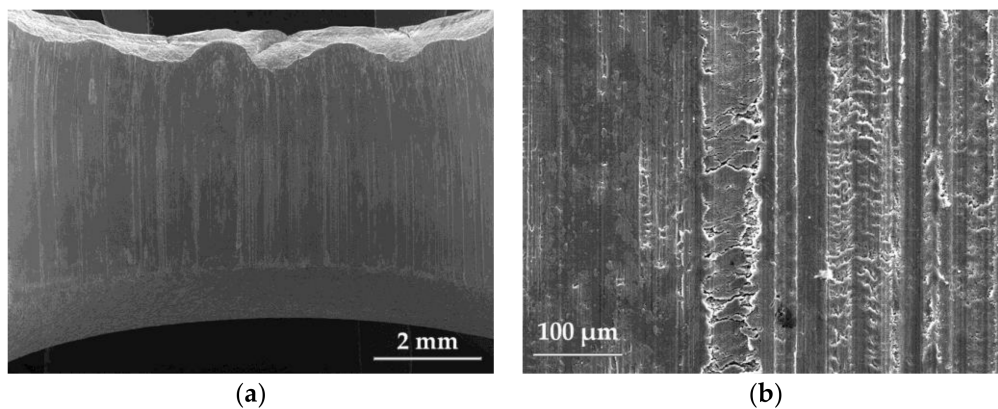


Figure 10. An EDX microanalysis of the punch surface coated by TiCN-MP after 120,000 strokes in selected areas: (a) point 1; (b) point 2; (c) point 3.

The punch surfaces, when considered worn due to galling of the processed material, are shown in Figure 11b,c. These were replaced in production by new ones, because of intensive scratches appearing on the hole surface (Figure 12).



**Figure 11.** The surface of the hole-flanging punch: (a) initial state (tool steel 1.3343); (b) tool steel after 20,000 strokes; (c) tool steel with the TiCN-MP coating after 120,000 strokes.



**Figure 12.** The surface of the hole after flanging with the TiCN coated punch after 120,000 strokes: (a) overall view; (b) detailed view.

### 3.3. Numerical Simulation of the Hole-Flanging Process

The simulation model of the hole-flanging process is shown in Figure 13a. The 3D models of the punch, die and blank holder were meshed as surfaces with a Rigid Body definition. The blank with the initial hole was meshed to hexahedron volume elements with a size of 0.35 mm in plane and with 5 layers in thickness. Based on the material parameters shown in Table 2, the Krupkowsky hardening model  $\sigma = 854 \times (0.00441 + \phi^{0.146})$  with an orthotropic Hill48 yield criterion were used. The contact conditions between the blank, punch and die were defined as dry friction based on Coulomb's law, with a friction coefficient of 0.3. A blank holder force of 100 kN was set to prevent material movement during the hole-flanging process.

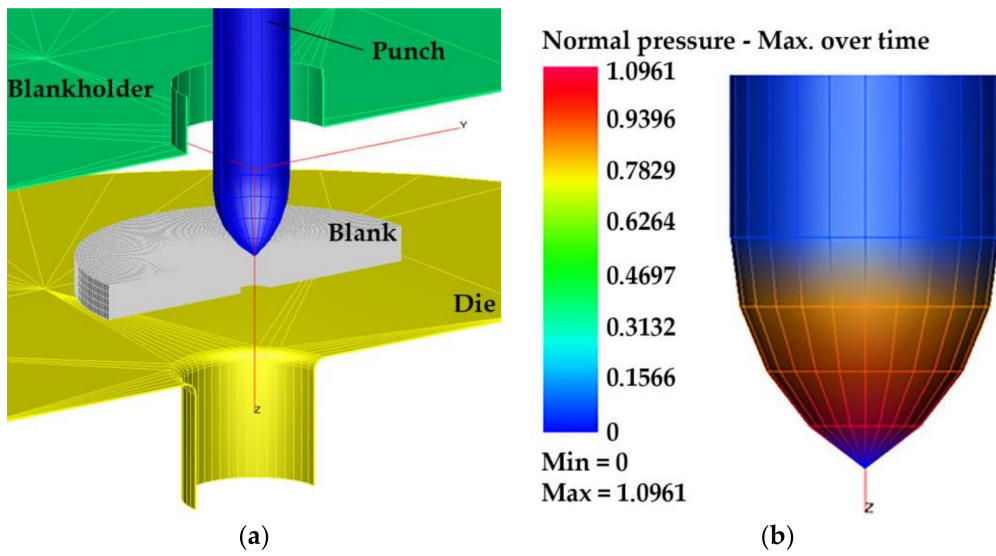


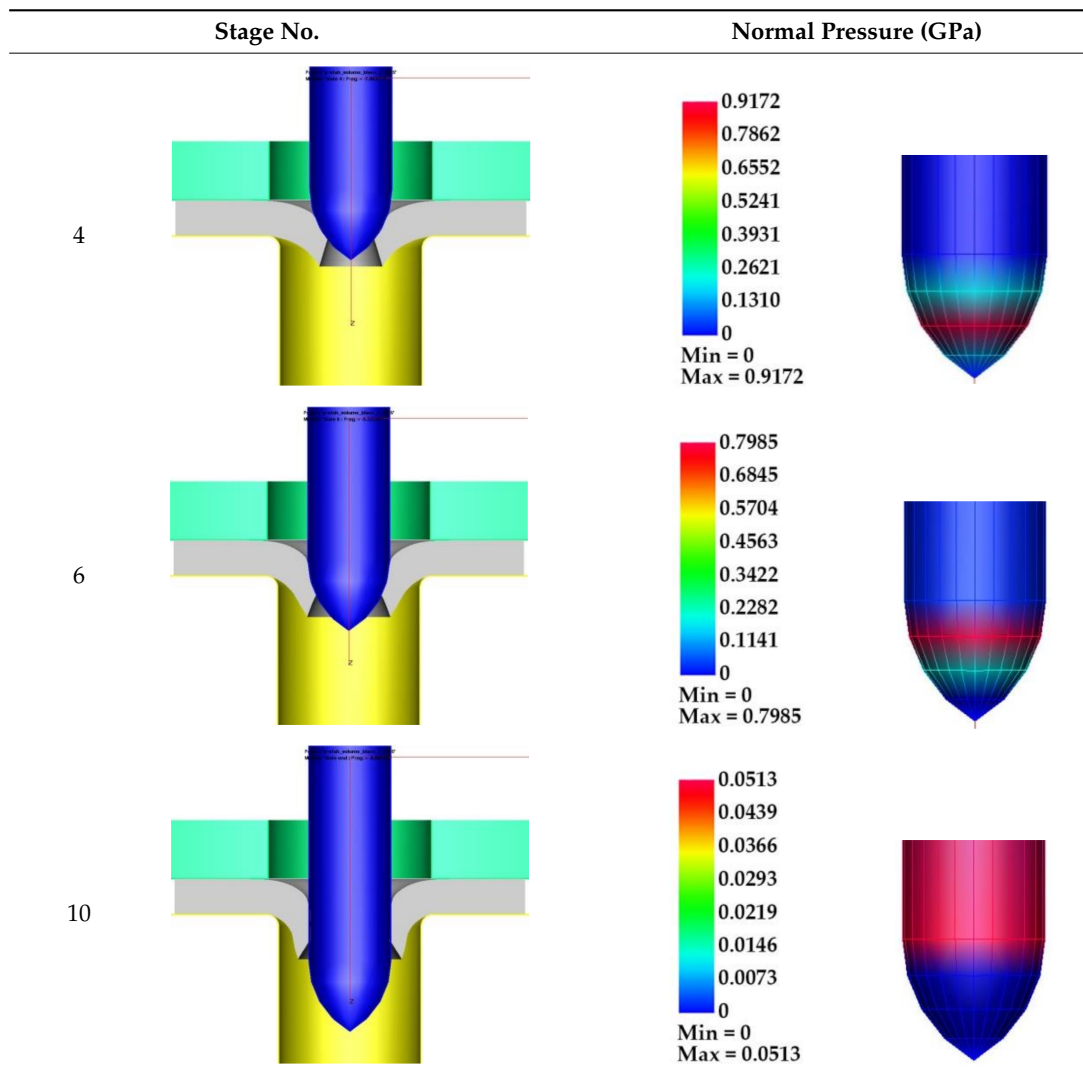
Figure 13. The simulation of the hole-flanging process: (a) simulation model; (b) normal pressure.

As a result of the numerical simulation, the normal pressure on the punch surface was evaluated (Figure 13b) in 10 stages during the punch path (Table 6).

Table 6. The hole-flanging process-results of the numerical simulation (selected stages).

Stage No.	Normal Pressure (GPa)
1	
2	

Table 6. Cont.



The hole creation during the hole-flanging, along with the normal pressure, is shown in Table 6 for selected stages. The maximal normal pressure was 1009 MPa in stage 2 and decreased slightly to 799 MPa in stage 6. Following this, contact pressure decreased rapidly until the hole was formed (stage 10). The dependence normal pressure based on the punch path is shown in Figure 14.

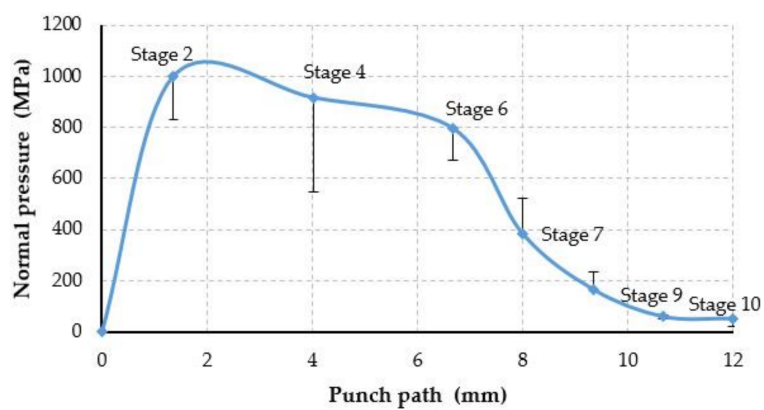


Figure 14. The dependence normal pressure based on the punch path during the hole-flanging process.

The normal pressure was also calculated for maximal and minimal friction coefficients measured via a Pin-On-Disc test (Table 5). The results are shown as error bars for a 95% confidence interval of the normal pressure calculated for different frictions. Thus, the highest values of the normal pressure during the hole-flanging process was found from stages 2 to 6, when the material was substantially deformed.

### 3.4. Discussion

The roughness of the punch after the coating via TiCN-MP decreased from 0.2  $\mu\text{m}$  (tool steel) to  $0.155 \pm 0.015 \mu\text{m}$ , as shown in Table 4. The decrease of roughness after the coating also had been found by [18] when TiAlCrN was applied. Based on [28,29], the coated punch was polished to remove droplets after the coating process. The friction coefficient measured by the Pin-On disc test decreased from 0.78 to 0.495 when the load increased. Sresommroeg reached almost the same value for TiCN-MP coating, and it is 1/3 lower when measured for hardened tool steel [35]. The thickness of the coating was 2.51  $\mu\text{m}$  and the average value of the indentation microhardness  $H_{IT}$  was 54 GPa. It is higher than when it is measured for this type of coating, but it depends on the C:N ratio during the deposition process [36]. The adhesion of the TiCN-MP coating to the substrate (hardened tool steel 1.3343) measured by the Scratch test has been shown to be very good.

From the view of tribology, contact between two bodies occurs through the limited portions of the peaks of opposing asperities when they are interacting. The real area of contact depends on the normal force and the yield pressure of the weaker material [37]. In our article, we consider these to be constant due to the fact that the same material is being processed (the weaker one) and that the same tool geometry is being used for the uncoated and coated punched. Thus, the real area of contact is considered, here, to be constant. Archards introduced the fact that the wear rate depends on the applied load, hardness of the sliding materials, sliding speed and constant, referred to as the wear coefficient [38]. While the applied load and sliding speed influence the wear rate, the hardness is inversely related to both of these. Thus, we assume a low wear rate when the materials with an increased hardness are in contact.

Based on contact mechanics, the type of contact should be described by the plasticity index  $\psi$ , involving such parameters as composite elastic modulus  $E$  (as a numerator), hardness  $H$  (as a denominator) and the square root of the ratio of the mean deviation of the surface asperity height  $\sigma^*$  to the mean asperity radius  $\beta$  [17,37,38]. The ratio  $\sigma^*/\beta$  is considered here to be constant, because the roughness of the uncoated and coated punches is almost the same. Thus, the type of contact is given by material properties: the composite elastic modulus and hardness. If the plasticity index  $\psi < 0.6$ , the contact should be an elastic one, and if  $\psi > 1$ , a part of the contact will involve a plastic flow. The values for the plasticity index  $>10$  are found when using typical values for the case of a hard coated tool contacting a soft steel sheet [39]. He also analytically proved the minor effect of an elastic modulus but the major effect of the hardness of coating, by increasing the hardness difference between the coated tool and the sheet. When considering the hardness of the TiCN-MP coating (54 GPa) and the hardness of the tool steel (61 HRC) (i.e., approx. 2.4 GPa) there is a huge difference. Sresommroeg experimentally confirmed the lower specific wear rate for TiCN coating via a ball-on disk test against cold rolled carbon steel [35]. Bull also found out that the carbon content is essential for maximizing the coating life and that the microhardness of coating mirrors the wear performance of PVD TiCN coatings in the ball-on-disc test [40].

From the point of view of contact physics and chemistry, adhesion is a result of interfacial molecular material interactions and surface forces [37]. Thus, the adhesion effect is influenced by the elasto-plastic contact behavior of the contact bodies (determining the size of the real area of contact), the influence of elastic stresses in contact separation and the presence of surface films and surface asperities. As was experimentally confirmed, it is described by an adhesion coefficient, and it has been proven that the adhesion coefficient decreases with increasing hardness (increasing elastic moduli and surface energy) and that it depends on the crystal structure [37].

Based on the production experiment and numerical simulation of the hole-flanging process, the adhesion of the base material to the punch surface appeared at the area of the highest normal contact pressure. By applying the TiCN-MP coating, the tool life increased approximately 6 times. We assume, as a consequence of improved friction, that this is due to droplets elimination, as well as to the increased hardness of the punch surface. Thus, well adhered TiCN-MP coating created the hard interlayer between tool steel and the material that was processed.

#### 4. Conclusions

Based on the results reached during the production experiment, the following findings have been stated:

- The distinctive wear of the punch made of tool steel 1.3343 hardened to 61 HRC has been shown after 7000 strokes. Detailed SEM and EDX analyses showed intensive galling of the processed material and its release by the tool movement, resulting in adhesive wear. The wear resulted from the 20,000 strokes, after which the punch was changed during production due to intensive scratches in the produced hole surface.
- The PVD coating TiCN-MP with a thickness of 2.51  $\mu\text{m}$  and a hardness  $H_{\text{IT}}$  of 54 GPa applied to the hardened tool steel has shown very good adhesion to the subsurface layers, as proven by the scratch test. The measured compression strain in coating  $\varepsilon = -0.017$  parallel to the surface assumes a good performance when the tensile stress is inducted parallel to the surface.
- The same level-of-wear of the coated punch, made of tool steel 1.3343 hardened to 61 HRC and coated by TiCN-MP, has been shown after 120,000 strokes. SEM and EDX analyses showed adhesive wear by galling of the processed material, located in the ogive area of the punch.
- A numerical simulation of the hole-flanging process identified the high level of normal contact pressure within 1096 to 796 MPa. The position of the high normal contact pressure is well correlated to the position of the adhesive wear for the uncoated and coated punches.

As was shown, by applying the TiCN-MP coating to the punch surface, the tool life was increased by approximately 6 times. This makes a substantial impact on the maintenance of the tool and production costs. The research was done for punch geometry known as tangent ogive and described by the CRH ratio = 0.98. Research to follow will focus on the change of CRH ratio and its influence on the normal pressure level and the wear of active hole-flanging punch surfaces.

**Acknowledgments:** The authors are grateful for the support of experimental works to Slovak Research and Development Agency, under projects APVV-0682-11, APVV-0273-12 and APVV-14-0834. We are also grateful to Grant Agency for the support of the project VEGA 2/0113/16.

**Author Contributions:** Emil Spišák and Miroslav Džupon conceived and designed the experiments; Miroslav Tomáš and Emil Evin performed the production experiments; Miroslav Džupon performed tests of coating and punches after wear; all authors analyzed the data; Miroslav Džupon and Miroslav Tomáš wrote the paper.

**Conflicts of Interest:** The authors declare no conflict of interest.

#### References

1. Hyun, D.I.; Oak, S.M.; Kang, S.S.; Moon, Y.H. Estimation of hole flangeability for high strength steel plates. *J. Mater. Process. Technol.* **2002**, *130–131*, 9–13. [[CrossRef](#)]
2. Thipprakmas, S.; Phanitwong, W. Finite element analysis of flange-forming direction in the hole flanging process. *Int. J. Adv. Manuf. Technol.* **2012**, *61*, 609–620. [[CrossRef](#)]
3. Cui, Z.; Gao, L. Studies on hole-flanging process using multistage incremental forming. *CIRP J. Manuf. Sci. Technol.* **2010**, *2*, 124–128. [[CrossRef](#)]
4. Centeno, G.; Silva, M.B.; Cristino, V.A.M.; Vallengano, C.; Martins, P.A.F. Hole-flanging by incremental sheet forming. *Int. J. Mach. Tools Manuf.* **2012**, *59*, 46–54. [[CrossRef](#)]
5. Ghoreishi, M.; Low, D.K.Y.; Li, L. Comparative statistical analysis of hole taper and circularity in laser percussion drilling. *Int. J. Mach. Tools Manuf.* **2002**, *42*, 985–995. [[CrossRef](#)]

6. Dubey, A.K.; Yadava, V. Laser beam machining—A review. *Int. J. Mach. Tools Manuf.* **2008**, *48*, 609–628. [[CrossRef](#)]
7. Stachowicz, F. Estimation of hole-flange ability for deep drawing steel sheets. *Arch. Civ. Mech. Eng.* **2008**, *8*, 167–172. [[CrossRef](#)]
8. Frańcz, W.; Stachowicz, F.; Trzepieciński, T. Investigations of thickness distribution in hole expanding of thin steel sheets. *Arch. Civ. Mech. Eng.* **2012**, *12*, 279–283. [[CrossRef](#)]
9. Krichen, A.; Kacem, A.; Hbaieb, M. Blank-holding effect on the hole-flanging process of sheet aluminum alloy. *J. Mater. Process. Technol.* **2011**, *211*, 619–626. [[CrossRef](#)]
10. Li, M.; VanTyne, C.J.; Moon, Y.H. The effect of mechanical properties on hole flangeability of stainless steel sheets. *J. Mech. Sci. Technol.* **2015**, *29*, 5233–5239. [[CrossRef](#)]
11. Heng-Sheng, L.; Chih-Wei, T. An investigation of cold extruding hollow flanged parts from sheet metals. *Int. J. Mach. Tools Manuf.* **2007**, *47*, 2133–2139. [[CrossRef](#)]
12. Huang, Y.M. An elasto-plastic finite element analysis of the sheet metal stretch flanging process. *Int. J. Adv. Manuf. Technol.* **2007**, *34*, 641–648. [[CrossRef](#)]
13. Thipprakmas, S.; Jin, M.; Murakawa, M. Study on flanged shapes in fineblanked-hole flanging process (FB-hole flanging process) using finite element method (FEM). *J. Mater. Process. Technol.* **2007**, 192–193, 128–133. [[CrossRef](#)]
14. Kacem, A.; Krichen, A.; Manach, P.Y. Prediction of damage in the hole-flanging process using a physically based approach. *Int. J. Damage Mech.* **2015**, *24*, 840–858. [[CrossRef](#)]
15. Masmoudi, N.; Soussi, H.; Krichen, A. Determination of an adequate geometry of the flanged hole to perform formed threads. *Int. J. Adv. Manuf. Technol.* **2017**, *92*, 547–560. [[CrossRef](#)]
16. Heng-Sheng, L.; Chien-Yu, L.; Chia-Hung, W. Hole flanging with cold extrusion on sheet metals by FE simulation. *Int. J. Mach. Tools Manuf.* **2007**, *47*, 168–174. [[CrossRef](#)]
17. Totten, G.E. *Handbook of Lubrication and Tribology—Vol. I Application and Maintenance*, 2nd ed.; CRC Press: Boca Raton, FL, USA, 2006; ISBN 978-0-8493-2095-8.
18. Choi, H.S.; Kim, S.G.; Seo, P.K.; Kim, B.M.; Cha, B.C.; Ko, D.C. Experimental Investigation on Galling Performance of Tool Steel in Stamping of UHSS Sheets. *Int. J. Precis. Eng. Manuf.* **2014**, *15*, 1101–1107. [[CrossRef](#)]
19. Evin, E.; Tomáš, M.; Výboch, J. Verification of friction models implemented in the program PAMSTAMP 2G by strip drawn test. In *Proceedings of the NEWTECH 2011: Advanced Manufacturing Engineering: The International Conference, Brno, Czech Republic, 14–15 September 2011*; University of Technology: Brno, Czech Republic, 2011; pp. 109–114, ISBN 978-80-214-4267-2.
20. Evin, E.; Tomáš, M.; Výrostek, M.; Výboch, J. Local tribological characteristics of steel sheets for microforming. *Key Eng. Mater.* **2014**, *586*, 116–119. [[CrossRef](#)]
21. Pereira, M.P.; Yan, W.; Rolfe, B.F. Contact pressure evolution and its relation to wear in sheet metal forming. *Wear* **2008**, *265*, 1687–1699. [[CrossRef](#)]
22. Gorscak, D.; Filetin, T.; Cackovic, D. Selection of Steels and Coatings for Cold-Work Tools. *Mater. Manuf. Process.* **2009**, *24*, 828–831. [[CrossRef](#)]
23. Groche, P.; Moeller, N.; Hoffmann, H.; Suh, J. Influence of gliding speed and contact pressure on the wear of forming tools. *Wear* **2011**, *271*, 2570–2578. [[CrossRef](#)]
24. Moravec, J. Increase of the operating life of active parts of cold-moulding tools. *Tehnicki Vjesnik* **2017**, *24*, 143–146. [[CrossRef](#)]
25. Clarysse, F.; Lauwerens, W.; Vermeulen, M. Tribological properties of PVD tool coatings in forming operations of steel sheet. *Wear* **2008**, *264*, 400–404. [[CrossRef](#)]
26. Silva, F.; Martinho, R.; Andrade, M.; Baptista, A.; Alexandre, R. Improving the Wear Resistance of Moulds for the Injection of Glass Fibre-Reinforced Plastics Using PVD Coatings: A Comparative Study. *Coatings* **2017**, *7*, 28. [[CrossRef](#)]
27. Li, H.; Rong, S.; Sun, P.; Wang, Q. Microstructure, Residual Stress, Corrosion and Wear Resistance of Vacuum Annealed TiCN/TiN/Ti Films Deposited on AZ31. *Metals* **2017**, *7*, 5. [[CrossRef](#)]
28. Rodríguez-Barrero, S.; Fernández-Larrinoa, J.; Azkona, I.; López de Lacalle, L.N.; Polvorosa, R. Enhanced Performance of Nanostructured Coatings for Drilling by Droplet Elimination. *Mater. Manuf. Process.* **2014**, *31*, 593–602. [[CrossRef](#)]

29. Fernández-Abia, A.I.; Barreiro, J.; López de Lacalle, L.N.; González-Madruga, D. Effect of mechanical pre-treatments in the behaviour of nanostructured PVD-coated tools in turning. *Int. J. Adv. Manuf. Technol.* **2014**, *73*, 1119–1132. [[CrossRef](#)]
30. Elosegui, I.; Alonso, U.; Lopez de Lacalle, L.N. PVD coatings for thread tapping of austempered ductile iron. *Int. J. Adv. Manuf. Technol.* **2017**, 2663–2672. [[CrossRef](#)]
31. Fernández-Valdivielso, A.; López de Lacalle, L.N.; Urbikain, G.; Rodriguez, A. Detecting the key geometrical features and grades of carbide inserts for the turning of nickel-based alloys concerning surface integrity. *J. Mech. Eng. Sci.* **2015**, *230*, 3725–3742. [[CrossRef](#)]
32. Bao, Y.; Zhang, N.; Yang, G. Theoretical approach in predicting perforation of aluminum alloy foam target against different ogive-nosed projectile. *Appl. Mech. Mater.* **2010**, *44–47*, 3060–3066. [[CrossRef](#)]
33. Sitek, M.; Stachowicz, F. An effect of punch geometry on a size of a hole contour burr (in Poland Wpływ geometrii stempla na stopien wywiniecia obrzeza otworu). *Rudy Metale* **2004**, *49*, 60–64.
34. Huang, Y.M.; Chien, K.H. Influence of Cone Semi-Angle on the Formability Limitation of the Hole-Flanging Process. *Int. J. Adv. Manuf. Technol.* **2002**, *19*, 597–606. [[CrossRef](#)]
35. Sresomroeng, B.; Premanond, V.; Kaewtatip, P.; Khantachawana, A.; Koga, N.; Watanabe, S. Anti-adhesion performance of various nitride and DLC films against high strength steel in metal forming operation. *Diam. Relat. Mater.* **2010**, *19*, 833–836. [[CrossRef](#)]
36. Bull, S.J.; Bhat, D.G.; Staita, M.H. Properties and performance of commercial TiCN coatings. Part 1: Coating architecture and hardness modelling. *Surf. Coat. Technol.* **2003**, *163–164*, 499–506. [[CrossRef](#)]
37. Czichos, H.; Habig, K.H. *Tribologie—Handbuch*, 4th ed.; Springer Vieweg: Wiesbaden, Germany, 2015; ISBN 978-3-8348-2236-9.
38. Bruce, R.W. *Handbook of Lubrication and Tribology, Volume II: Theory and Design*, 2nd ed.; CRC Press: Boca Raton, FL, USA, 2006; ISBN 978-1420069082.
39. De Rooij, M.B. Tribological Aspects of Unlubricated Deep Drawing Processes. Ph.D. Thesis, University of Twente, Enschede, The Netherlands, 1998.
40. Bull, S.J.; Bhat, D.G.; Staita, M.H. Properties and performance of commercial TiCN coatings. Part 2: Tribological performance. *Surf. Coat. Technol.* **2003**, *163–164*, 507–514. [[CrossRef](#)]



© 2018 by the authors. Licensee MDPI, Basel, Switzerland. This article is an open access article distributed under the terms and conditions of the Creative Commons Attribution (CC BY) license (<http://creativecommons.org/licenses/by/4.0/>).